ARTICLE   **Open Access**

Unidentified major p-type source in SnSe: Multivacancies

Van Quang Nguyen[1,7], Thi Ly Trinh[1], Cheng Chang[2,3], Li-Dong Zhao[2], Thi Huong Nguyen[1,4], Van Thiet Duong[1], Anh Tuan Duong[5], Jong Ho Park[6], Sudong Park[6], Jungdae Kim[1] and Sunglae Cho[1]

Abstract

Tin selenide (SnSe) is considered a robust candidate for thermoelectric applications due to its very high thermoelectric figure of merit, ZT, with values of 2.6 in p-type and 2.8 in n-type single crystals. Sn has been replaced with various lower group dopants to achieve successful p-type doping in SnSe with high ZT values. A known, facile, and powerful alternative way to introduce a hole carrier is to use a natural single Sn vacancy, V_{Sn}. Through transport and scanning tunneling microscopy studies, we discovered that V_{Sn} are dominant in high-quality (slow cooling rate) SnSe single crystals, while multiple vacancies, V_{multi}, are dominant in low-quality (high cooling rate) single crystals. Surprisingly, both V_{Sn} and V_{multi} help to increase the power factors of SnSe, whereas samples with dominant V_{Sn} have superior thermoelectric properties in SnSe single crystals. Additionally, the observation that V_{multi} are good p-type sources observed in relatively low-quality single crystals is useful in thermoelectric applications because polycrystalline SnSe can be used due to its mechanical strength; this substance is usually fabricated at very high cooling speeds.

Introduction

The efficiency of thermoelectric devices is evaluated by the dimensionless figure of merit of the material, $ZT = S^2\sigma T/\kappa$, where S is the Seebeck coefficient, σ is the electrical conductivity, κ is the total thermal conductivity, and T is the absolute temperature. σ, S, and κ are interdependent quantities. To date, effort has been made to enhance ZT by increasing the power factor ($PF = S^2\sigma$) by band engineering[1–3] and by reducing κ by increasing the phonon scattering centers in superlattices, alloys, nanowires, nanotubes, other nanostructures[2] and mixed phase structures[4–6] such as nanostructured Bi_2Te_3[7], Na-doped $PbTe$[8] ($PbSe$[9]), and Bi_2Te_3/Sb_2Te_3 superlattices[10]. However, these state-of-the-art thermoelectric materials contain elements that are rare and toxic. Therefore, over the past few decades, researchers have focused on finding alternative thermoelectric materials that are economically and environmentally friendly. In addition, controlling the intrinsic point defects in a semiconductor is an important strategy for tuning its electronic and thermoelectric properties. Since the defect chemistry in a semiconductor is dependent on both its intrinsic properties and its external conditions, controlling point defects to enhance thermoelectric performance is challenging[11]. It has been reported that Ag dopants help to suppress Te vacancies due to the increase in electron chemical potential, while Na dopants help to enhance the hole concentration in p-type PbTe, leading to an enhancement in PF and a simultaneous reduction in thermal conductivity[12]. The number of intrinsic vacancies can be controlled by tuning their formation energy. The Ge vacancy concentration and distribution have been successfully controlled by introducing Cr dopants into the GeTe matrix, which helps to reduce the Ge vacancy formation energy, while the carrier concentration remains optimized[13]. Similarly, the generation of many Sn vacancies in p-type SnTe has been successfully suppressed by Pb alloying to enhance the defect formation energy[14]. The vacancy concentration in

Correspondence: Jungdae Kim (kimjd@ulsan.ac.kr) or
Sunglae Cho (slcho@ulsan.ac.kr)
[1]Department of Physics and Energy Harvest Storage Research Center,
University of Ulsan, Ulsan 44610, Republic of Korea
[2]School of Materials Science and Engineering, Beihang University, Beijing
100191, China
Full list of author information is available at the end of the article

half-Heuslers has also been controlled using doping/alloying experiments, whereas different dopants lead to different vacancy concentrations[15].

Since the report of ZT = 2.6 in p-type SnSe[16], SnSe has attracted significant attention. The high thermoelectric performance of undoped SnSe is attributed to its ultralow κ (< 0.4 Wm^{-1}K^{-1} at 923 K) caused by the strong anharmonicity of its chemical bonds[17,18]. The most frequently used method of optimizing the carrier concentration of SnSe has been to replace Sn with various dopants (substitution). For p-type SnSe, alkali metals (e.g., Na[19–21] and K[22]), I–B group metals (e.g., Ag[4,20,23]), and III-A group metals (e.g., In[24]) were used as acceptors. Recently, carbon fiber has been used to decouple the electrical and thermal transport in p-type polycrystalline SnSe, resulting in a ZT value of 1.3 at 823 K[25]. For n-type SnSe, V–A group metals (e.g., Bi[26,27]) and halogens (e.g., Cl, Br, and I[5,28,29]) were used as donors. However, it is fairly difficult to dope SnSe due to its anharmonic bonds[4]. The difficulty in doping SnSe limits the potential to explore its higher thermoelectric performance[30]. Thus far, it is still difficult to use SnSe in practical applications since the high cost production, weak mechanical and cleavable properties of SnSe single crystals, and the low performance of polycrystalline SnSe are attributed to the presence of a SnO_2 layer at the grain boundary[31].

It is well known that SnSe intrinsically shows a p-type character. Our previous studies confirmed that the p-type nature of SnSe is attributed to a single Sn vacancy (V_{Sn}), implying that V_{Sn} works as a hole provider[32–35]. We speculated that the growth speed can control the quality of the samples, i.e., the number of material defects, and thus control the natural amount of V_{Sn} during the growth process. A systematic study on intrinsic defects in SnSe is necessary for optimum thermoelectric performance, which should be done in single crystal form. SnSe single crystals have been fabricated at various growth speeds by changing the cooling rate near the melting point of SnSe (861 °C) from 0.5 to 5 °C/h during growth using a temperature gradient technique[27]. We found that as the cooling rate increased, the dominant defect changed from a V_{Sn} at cooling rates of 0.5 and 1 °C/h to multiple vacancies, V_{multi}, containing more than one Sn (Se) atom missing, at cooling rates of 2–5 °C/h. Surprisingly, not only V_{Sn}-dominant samples but also V_{multi}-dominant samples showed p-type conduction with PFs comparable to those in previous reports[16,27]. Based on our results, the slow cooling rate is beneficial for the thermoelectric performance of SnSe single crystals.

The polycrystalline SnSe has high mechanical strength and can be used in thermoelectric applications. The observation that the V_{multi} are good p-type sources in high cooling rate SnSe crystals is really important information for the thermoelectric application because polycrystalline SnSe which is usually fabricated at very high cooling rates can be used due to its high mechanical strength.

Materials and methods
Sample preparation

The SnSe samples were synthesized by a temperature gradient technique by heating the raw materials to 500 °C over 32 h and then to 950 °C over 45 h, soaking at this temperature for 15 h, cooling to 900 °C over 10 h, then cooling to 800 °C across the melting point of SnSe (861 °C) at various cooling rates (0.5, 1, 2, 3, 4, and 5 °C/h), and finally cooling to room temperature over 100 h. We used a slow heating rate to prevent explosion due to the high vapor pressure of Se.

Sample characterizations

We determined the carrier concentrations of the samples using a four-probe method. The values of σ and S were measured from 300 to 923 K using a ULVAC-RIKO ZEM3 system. The thermal diffusivities, D, were measured with a Netzsch LFA-457 (Germany) MicroFlash apparatus. The heat capacities, C_p, were obtained from ref. [11]. The values of κ were calculated using the formula $\kappa = DC_p\rho$, where ρ is the mass density (measured by the Archimedes method). STM was conducted at 79 K with an in situ cleaving technique. X-ray diffraction (XRD), field emission scanning electron spectroscopy (FE-SEM), and electron probe microanalyzer experiments were used to investigate the structure, composition, and morphology of the samples.

Results and discussion
Structural characterization

Figure 1a shows a photo of SnSe, which can be easily cleaved along the (*bc*) plane due to weak interlayer bonding. Our samples exhibit a lamellar microstructure, as shown in FE-SEM images (see Fig. S1a). Room temperature X-ray diffraction (XRD) patterns of cleaved planes of SnSe single crystals are shown in Fig. 1b, where all diffraction peaks can be indexed corresponding to the orthorhombic SnSe phase (space group Pnma). Only sharp (h00) peaks are observed, indicating the high crystallinity of our samples with the cleaved plane perpendicular to the *a*-axis. The lattice parameters of the samples were determined using powder XRD and are listed in Table 1.

Thermoelectric transport studies

Figure 2a–c shows the temperature dependence of σ, S, and PF of various SnSe single crystals prepared at 6 different cooling rates. All the samples had similar σ values in the mid-temperature range, while their σ values differed in the low- and high-temperature ranges. At temperatures ranging from 300 to 570 K, the σ of samples
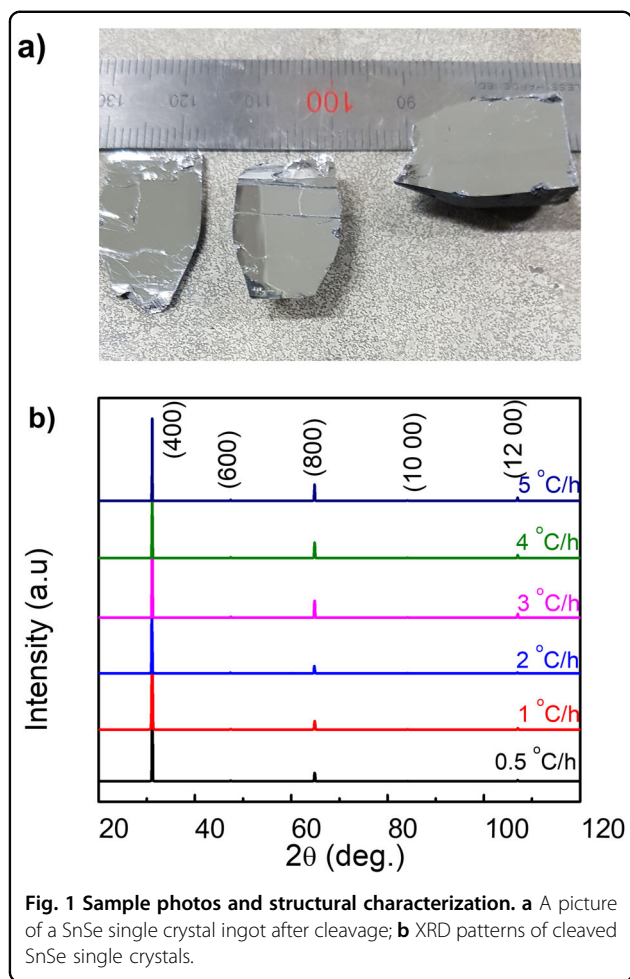
Fig. 1 Sample photos and structural characterization. a A picture of a SnSe single crystal ingot after cleavage; **b** XRD patterns of cleaved SnSe single crystals.

Table 1 Room temperature lattice constants and carrier concentration of samples grown at various cooling rates.

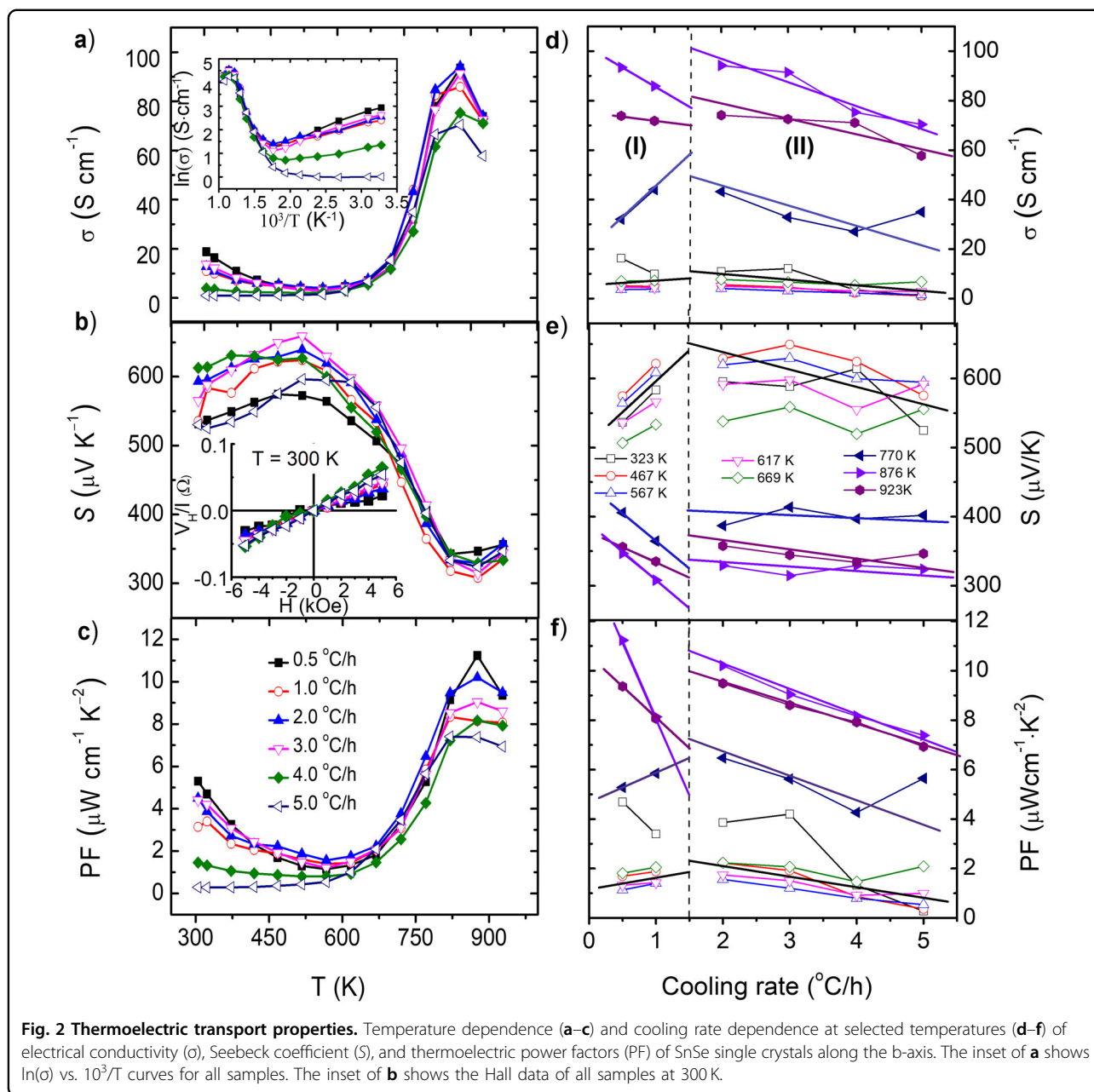| Sample (cooling rate, °C/h)	a (Å)	b (Å)	c (Å)	Volume (Å)^3	Carrier density at 300 K ($\times 10^{17}$)
0.5	11.474	4.729	4.177	226.646	5.53
1	11.478	4.730	4.180	226.923	3.95
2	11.477	4.730	4.178	226.821	2.20
3	11.477	4.728	4.178	226.711	1.84
4	11.472	4.728	4.177	226.577	2.16
5	11.475	4.730	4.177	226.698	1.61

prepared at 5 °C/h increased with temperature, while those of other samples decreased. Above 570 K, σ of all the samples increased up to ~800 K, reached a maximum value at 876 K, and then decreased with temperature. The maximum σ values were 93.5, 85.8, 94.2, 91.4, 75.3, and 70.4 S cm^{-1} for samples prepared with cooling rates of

0.5, 1, 2, 3, 4, and 5 °C/h, respectively, comparable to the reported value ($\sim$ 85 S cm^{-1})[17]. The ln(σ) vs. 10^3/T curves of all samples showed two different slopes. The sample prepared with a cooling rate of 5 °C/h had two different negative slopes, while the other samples had positive slopes below 570 K and negative slopes above 570 K, indicating the complex activation energies of the carriers. These variations in σ vs. temperature up to 800 K were attributed to complex thermally activated carriers and/or activation energies or carrier mobilities. The behavior of σ above 800 K was attributed to the phase transition from Pnma ($E_g = 0.829$ eV) to Cmcm ($E_g = 0.464$ eV).

All samples had positive S values over the whole temperature range, indicating dominant hole conduction. The value of S increased with increasing temperature up to 520 K, then decreased as the temperature was increased to 876 K, and finally increased again at temperatures above 876 K (Fig. 2b). This behavior of S is consistent with that of σ. The S values of all samples also deviated in the low temperature range (530–612 µV/K at 300 K) but were more consistent at higher temperatures. The positive hole conduction behavior was confirmed by Hall measurements, with a carrier concentration level of 10^{17} cm^{-3} at room temperature for all samples (inset of Fig. 2b, Fig. S7a, and Table 1).

The calculated PF showed a similar temperature dependence on σ (Fig. 2c). Deviating PF values were obtained at low and high temperature ranges, while closer PF values were obtained in the middle temperature range. The obtained maximum PF values were 11.2, 8.1, 10.2, 9.0, 8.2, and 7.4 µWcm^{-1}K^{-2} at 876 K for samples prepared with cooling rates of 0.5, 1, 2, 3, 4, and 5 °C/h, respectively, comparable to the reported value (10.1 µWcm^{-1}K^{-2})[17]. The samples prepared at 0.5 and 2 °C/h had similar values.

To clarify the influence of the cooling rate on transport properties, we plotted the cooling-rate-dependent transport parameters at selected temperatures, as shown in Fig. 2d–f. The cooling rate had less effect on σ at 567, 617, and 669 K. At low and high temperatures (< 567 K and > 669 K), σ varied differently with cooling rate for samples with cooling rates ≤ 1 °C/h (region I) vs. > 2 °C/h (region II). In Fig. 2d–f, these two regions are separated by a black dashed line. The value of S had a strong cooling rate dependence at low temperatures and a lower cooling rate dependence at moderate and high temperatures. S also varied differently with cooling rate in regions I and II. As a result, the calculated PFs exhibited two distinct trends with cooling rate. The cooling rate had a strong effect on the PFs at low and high temperatures, while it had less of an effect at intermediate temperatures. These observations indicate a discontinuity in the transport parameters vs. cooling rate. To verify these results, we grew five different single crystals at a cooling rate of 1 °C/h and studied their transport properties (Fig. S2). These samples

Fig. 2 Thermoelectric transport properties. Temperature dependence (**a–c**) and cooling rate dependence at selected temperatures (**d–f**) of electrical conductivity (σ), Seebeck coefficient (S), and thermoelectric power factors (PF) of SnSe single crystals along the b-axis. The inset of **a** shows ln(σ) vs. $10^3/T$ curves for all samples. The inset of **b** shows the Hall data of all samples at 300 K.
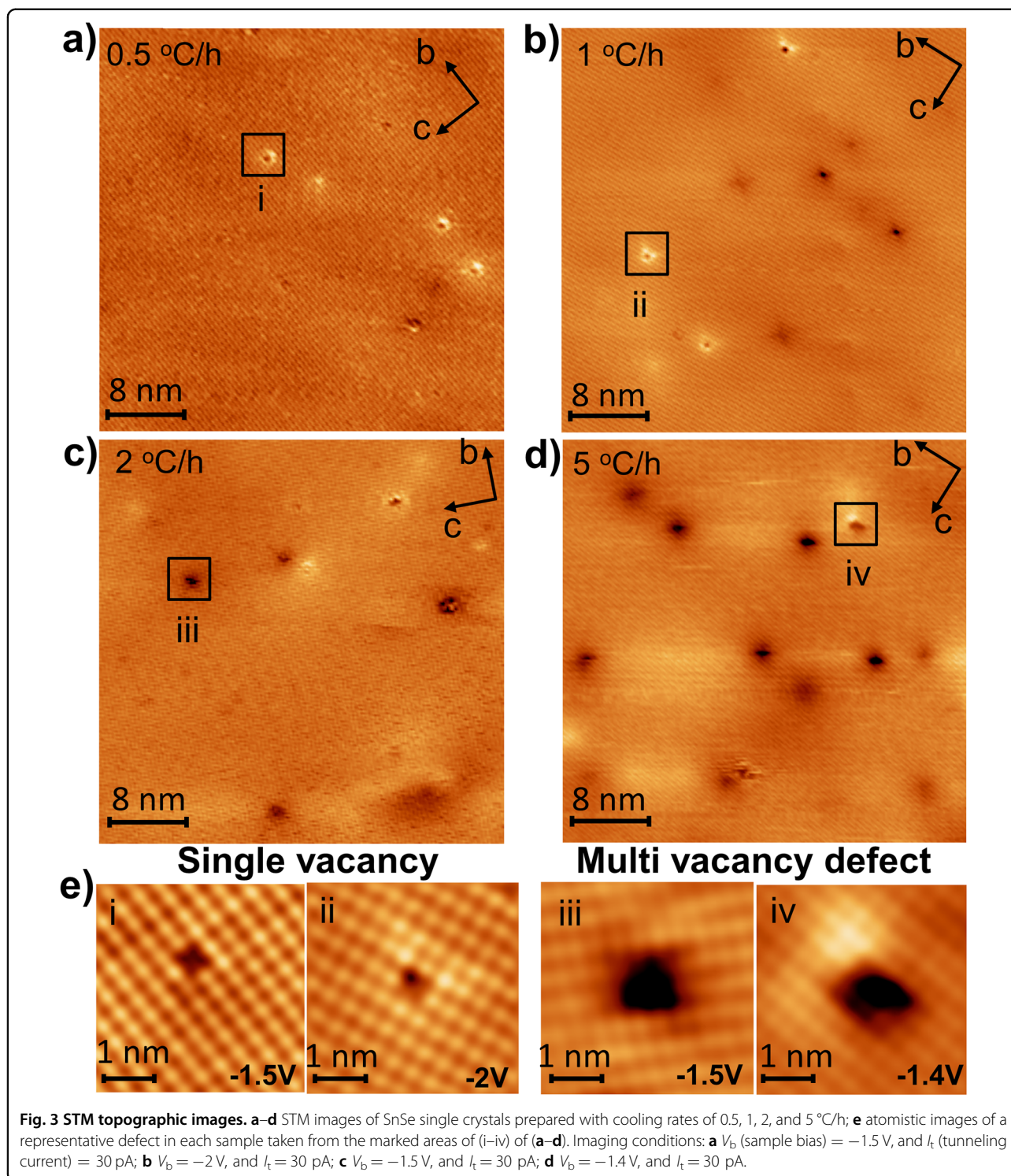
confirmed the presence of the discontinuity in transport vs. cooling rate in SnSe single crystals, as clearly denoted by the solid lines in the figures.

STM microscopic studies

To understand the discontinuity behavior in transport data, we conducted scanning tunneling microscopy (STM) measurements to investigate the defect characteristics of these samples. All samples were exfoliated inside an ultrahigh vacuum chamber to obtain clean surfaces for STM analysis. All STM analyses were conducted at 79 K. Figure 3a–d shows STM images taken

from the same samples with cooling rates of 0.5, 1, 2, and 5 °C/h. Many defects were observed in all samples, as shown in Fig. 3a–d. Intriguingly, the nature of the defects differed strikingly between the samples in region I (cooling rate of 0.5–1 °C/h) and region II (cooling rate of 2–5 °C/h). V_{Sn} is usually known to be dominant among various types of defects, and V_{Sn} is also responsible for the p-type characteristic of SnSe[32]. Indeed, V_{Sn} is predominantly observed in the samples prepared with a cooling rate of 0.5–1 °C/h. Figure 3e(i, ii) shows atomistic images of representative V_{Sn} instances taken from the marked areas of (i, ii) in Fig. 3a,b. In the STM topography,

Fig. 3 STM topographic images. a–d STM images of SnSe single crystals prepared with cooling rates of 0.5, 1, 2, and 5 °C/h; **e** atomistic images of a representative defect in each sample taken from the marked areas of (i–iv) of (**a–d**). Imaging conditions: **a** V_b (sample bias) = −1.5 V, and I_t (tunneling current) = 30 pA; **b** V_b = −2 V, and I_t = 30 pA; **c** V_b = −1.5 V, and I_t = 30 pA; **d** V_b = −1.4 V, and I_t = 30 pA.

Sn atoms were visible as bright spots, while Se atoms were located in dark regions and were not visible[32].

Interestingly, the samples prepared at 2–5 °C/h (region II) revealed a very different defect nature in which the dominant defects were complex vacancies consisting of more than one Sn atom vacancy. These instances of V_{multi}

were present in various sizes and shapes, as shown in Fig. 3e (iii, iv), taken from area (iii, iv) in Fig. 3c, d. More examples of those defects in the region I and II samples are also provided in Fig. S5. With the increase in solidification speed (cooling rate) above 2 °C/h, multi-vacancies are dominant, and the size of the multi-vacancies

increases. We conclude that the electrical properties of the region II samples were mainly caused by V_{multi}, while V_{Sn} played the major role in the region I samples. Therefore, the discontinuity observed in the transport in Fig. 2 was attributed to the change in defect characteristics from V_{Sn} in high-quality single crystals (region I) to V_{multi} in relatively low-quality single crystals (region II). As shown in Fig. 2, the region II samples had p-type PF values ($10.2 \, \mu\text{Wcm}^{-1}\text{K}^{-2}$) that were comparable to those of the region I samples ($11.2 \, \mu\text{Wcm}^{-1}\text{K}^{-2}$), indicating that the V_{multi}, dominant in the region II samples, also worked as a good acceptors for producing the hole carriers required for thermoelectric performance.

Conclusions

We introduced an alternative, facile, and much more powerful method via the engineering of vacancies to introduce hole carriers in SnSe. With the help of transport and STM studies, we discovered that V_{Sn} are dominant in high-quality SnSe single crystals, while V_{multi} are dominant in low-quality single crystals. Surprisingly, both V_{Sn} and V_{multi} are good p-type sources in SnSe with comparable PF values. The V_{multi} become the dominant and p-type source when the cooling rate increases, which is expected in polycrystalline SnSe. This information provides a deeper understanding of the nature of the defects in SnSe.

Author details
^{1}Department of Physics and Energy Harvest Storage Research Center, University of Ulsan, Ulsan 44610, Republic of Korea. ^{2}School of Materials Science and Engineering, Beihang University, Beijing 100191, China. ^{3}Institute of Science and Technology Austria, Am Campus 1, 3400 Klosterneuburg, Austria. ^{4}Department of Applied Physics, Integrated Education Institute for Frontier Science and Technology (BK21 Four) and Institute of Natural Sciences, Kyung Hee University, Yongin 17104, Republic of Korea. ^{5}Phenikaa Research and Technology Institute, A&A Green Phoenix Group, 167 Hoang Ngan, Hanoi 10000, Vietnam. ^{6}Thermoelectric Conversion Research Center, Korea Electrotechnology Research Institute (KERI), Changwon 51543, Republic of Korea. ^{7}Present address: Neutron Science Division, Korea Atomic Energy Research Institute, Daejeon 34057, Republic of Korea

Author contributions
V.Q.N., T.H.N., and V.T.D. synthesized the single crystals and characterized the carrier concentration. V.Q.N., A.T.D., and S.C. determined the crystal structure. C.C., L.D.Z., J.H.P., and S.D.P. measured the thermoelectric transport and thermal diffusivity. T.T.L. and J.K. conducted the STM experiments. S.C. and J.K. initiated the study and edited the manuscript. V.Q.N. wrote the paper with discussions and comments from all the authors. S.C. supervised the project.

Conflict of interest
The authors declare no conflict of interest.

Publisher's note
Springer Nature remains neutral with regard to jurisdictional claims in published maps and institutional affiliations.

References
1. Liu, W. et al. Convergence of conduction bands as a means of enhancing thermoelectric performance of n-type $Mg_2Si_{1-x}Sn_x$ solid solutions. *Phys. Rev. Lett.* **108**, 1–5 (2012).
2. Pei, Y. et al. Convergence of electronic bands for high performance bulk thermoelectrics. *Nature* **473**, 66–69 (2011).
3. Girard, S. N. et al. High performance Na-doped PbTe–PbS thermoelectric materials: Electronic density of states modification and shape-controlled nanostructures. *J. Am. Chem. Soc.* **133**, 16588–16597 (2011).
4. Chen, C.-L., Wang, H., Chen, Y.-Y., Day, T. & Snyder, G. J. Thermoelectric properties of p-type polycrystalline SnSe doped with Ag. *J. Mater. Chem. A* **2**, 11171–11176 (2014).
5. Zhang, Q. et al. Studies on Thermoelectric Properties of n-type Polycrystalline $SnSe_{1-x}S_x$ by Iodine Doping. *Adv. Energy Mater.* **5**, 1–8 (2015).
6. Tang, G. et al. Rock-salt-type nanoprecipitates lead to high thermoelectric performance in undoped polycrystalline SnSe. *RSC Adv.* **7**, 8258–8263 (2017).
7. Son, J. S. et al. N-type nanostructured thermoelectric materials prepared from chemically synthesized ultrathin Bi_2Te_3 nanoplates. *Nano Lett.* **12**, 640–647 (2012).
8. Jood, P. et al. Na doping in PbTe-solubility, band convergence, phase boundary mapping, and thermoelectric properties. *J. Am. Chem. Soc.* **142**, 15464–15475 (2020).
9. Wang, H., Pei, Y., Lalonde, A. D. & Snyder, G. J. Heavily doped p-type PbSe with high thermoelectric performance: An alternative for PbTe. *Adv. Mater.* **23**, 1366–1370 (2011).
10. Venkatasubramanian, R., Siivola, E., Colpitts, T. & O'Quinn, B. Thin-film thermoelectric devices with high room-temperature figures of merit. *Nature* **413**, 597–602 (2001).
11. Liu, Z. Shaping the role of germanium vacancies in germanium telluride: Metastable cubic structure stabilization, band structure modification, and stable N-type conduction. *NPG Asia Mater.* **12**, 66 (2020).
12. Jang, H. et al. Regulating Te vacancies through dopant balancing via excess Ag enables rebounding power factor and high thermoelectric performance in p-type PbTe. *Adv. Sci.* **8**, 2100895 (2021).
13. Shuai, J., Sun, Y., Tan, X. & Mori, T. Manipulating the Ge vacancies and Ge precipitates through Cr doping for realizing the high-performance GeTe thermoelectric material. *Small* **16**, 1906921 (2020).
14. Pang, H. et al. Realizing N-type SnTe thermoelectrics with competitive performance through suppressing Sn vacancies. *J. Am. Chem. Soc.* **143**, 8538–8542 (2021).
15. Maclaren, D. A. & Bos, J. G. Low thermal conductivity and promising thermoelectric performance in A_xCoSb (A = V, Nb or Ta) half-Heuslers with inherent vacancies. *J. Mater. Chem. C* **7**, 6539–6547 (2019).
16. Zhao, L.-D. et al. Ultralow thermal conductivity and high thermoelectric figure of merit in SnSe crystals. *Nature* **508**, 373–377 (2014).
17. Lee, S. et al. Resonant bonding leads to low lattice thermal conductivity. *Nat. Commun.* **5**, 1–8 (2014).
18. Li, C. W. et al. Orbitally driven giant phonon anharmonicity in SnSe. *Nat. Phys.* **11**, 1063–1069 (2015).
19. Zhao, L. et al. Ultrahigh power factor and thermoelectric performance in hole-doped single-crystal SnSe. *Science* **351**, 141–144 (2016).
20. Peng, K. et al. Broad temperature plateau for high ZTs in heavily doped p-type SnSe single crystals. *Energy Environ. Sci.* **9**, 454–460 (2016).
21. Wei, T.-R. et al. Thermoelectric transport properties of pristine and Na-doped $SnSe_{1-x}Te_x$ polycrystals. *Phys. Chem. Chem. Phys.* **17**, 30102–30109 (2015).
22. Wei, T. R. et al. Distinct impact of alkali-ion doping on electrical transport properties of thermoelectric p-type polycrystalline SnSe. *J. Am. Chem. Soc.* **138**, 8875–8882 (2016).
23. Jin, M. et al. Single crystal growth of $Sn_{0.97}Ag_{0.03}Se$ by a novel horizontal Bridgman method and its thermoelectric properties. *J. Cryst. Growth* **460**, 112–116 (2017).
24. Kim, J. H. et al. Indium substitution effect on thermoelectric and optical properties of $Sn_{1-x}In_xSe$ compounds. *J. Alloy. Compd.* **682**, 785–790 (2016).

25. Yang, G. et al. Enhancing the thermoelectric performance of polycrystalline SnSe by decoupling electrical and thermal transport through carbon fiber incorporation. *ACS Appl. Mater. Interfaces* **12**, 12910–12918 (2020).

26. Nguyen, V. Q. et al. Thermoelectric properties of hot-pressed Bi-doped n-type polycrystalline SnSe. *Nanoscale Res. Lett.* **13**, 4–10 (2018).

27. Duong, A. T. et al. Achieving ZT=2.2 with Bi-doped n-type SnSe single crystals. *Nat. Commun.* **7**, 1–6 (2016).

28. Wang, X. et al. Optimization of thermoelectric properties in n-type SnSe doped with BiCl₃. *Appl. Phys. Lett.* **108**, 1–6 (2016).

29. Chang, C. et al. Raising thermoelectric performance of n-type SnSe via Br doping and Pb alloying. *RSC Adv.* **6**, 98216–98220 (2016).

30. Xiao, Y. & Zhao, L. D. Seeking new, highly effective thermoelectrics. *Science* **367**, 1196–1197 (2020).

31. Zhou, C. et al. Polycrystalline SnSe with a thermoelectric figure of merit greater than the single crystal. *Nat. Mater.* **20**, 1378–1384 (2021).

32. Duvjir, G. et al. Origin of p-type characteristics in a SnSe single crystal. *Appl. Phys. Lett.* **110**, 262106 (2017).

33. Wu, D. et al. Direct observation of vast off -stoichiometric defects in single crystalline SnSe. *Nano Energy* **35**, 321–330 (2017).

34. Zhou, Y. et al. Influence of defects on the thermoelectricity in SnSe: A comprehensive theoretical study. *Phys. Rev. B* **97**, 1–8 (2018).

35. Huang, Y. et al. First-principles study on intrinsic defects of SnSe. *RSC Adv.* **7**, 27612–27618 (2017).